

Analytical Methods

Accepted Manuscript



This is an *Accepted Manuscript*, which has been through the Royal Society of Chemistry peer review process and has been accepted for publication.

Accepted Manuscripts are published online shortly after acceptance, before technical editing, formatting and proof reading. Using this free service, authors can make their results available to the community, in citable form, before we publish the edited article. We will replace this *Accepted Manuscript* with the edited and formatted *Advance Article* as soon as it is available.

You can find more information about *Accepted Manuscripts* in the [Information for Authors](#).

Please note that technical editing may introduce minor changes to the text and/or graphics, which may alter content. The journal's standard [Terms & Conditions](#) and the [Ethical guidelines](#) still apply. In no event shall the Royal Society of Chemistry be held responsible for any errors or omissions in this *Accepted Manuscript* or any consequences arising from the use of any information it contains.

1
2
3
4 **Design of a miniaturized multisensor chip with nanoband electrode**
5
6 **array and light addressable potentiometric sensor for ion sensing**
7

8 Hao Wan, Qiyong Sun, Haibo Li, Fei Sun, Ning Hu*, Ping Wang*
9

10
11 *Biosensor National Special Laboratory, Department of Biomedical Engineering, Zhejiang*
12

13
14 *University, Hangzhou, 310027, P. R. China*
15

16
17 **Corresponding authors:*
18

19 *E-mail address: cnpwang@zju.edu.cn (Ping Wang), huning@zju.edu.cn (Ning Hu)*
20

21
22 *Tel: +86 571 87952832*
23
24
25
26
27
28
29
30
31
32
33
34
35
36
37
38
39
40
41
42
43
44
45
46
47
48
49
50
51
52
53
54
55
56
57
58
59
60

Abstract

In this paper, we present a novel miniaturized multisensor chip integrated with nanoband electrode array (NEA) for lead and copper detection and light addressable potentiometric sensor (LAPS) for pH sensing. By this means, pH information could be provided before electrochemical analysis to ensure high performance in heavy metal quantification due to significant effects of the solution acidity on electrochemical analysis. The fabrication processes of the multisensor chip were detailed. Electrochemical behaviour of NEA was characterized by cyclic voltammetry in sulfuric acid and acetate buffer. As to detect lead and copper qualitatively and quantitatively, square wave anodic stripping voltammetry (SWASV) was applied with standard addition method. Deposition potential and deposition time were respectively optimized to be -0.6 V and 120 s. The NEA exhibited a sensitivity of 0.510 $\mu\text{A}/\text{ppb}$ and 0.678 $\mu\text{A}/\text{ppb}$ towards lead and copper with high correlation coefficients. The repetitive and long-term experiments also demonstrated good reproducibility and stability of NEA in heavy metal detection. On the other hand, the silicon nitride modified LAPS showed a pH sensitivity of 56.49 mV/pH with high correlation coefficient of 0.9999. Reproducibility of LAPS was also investigated with deviation less than 2 mV in both two samples. The results indicate that the miniaturized multisensor chip demonstrates good electrochemical performance in heavy metal and pH sensing.

Keywords: Multisensor chip; Nanoband electrode array (NEA); Light addressable potentiometric sensor (LAPS); Heavy metal detection;

1. Introduction

Heavy metals contamination, mainly deriving from discharge of manufacturing industry has received extensive social concerns owing to their severe hazards to human health. For instance, excessive intake of lead causes neurological, neurobehavioral, hematological and renal diseases, especially potentially harmful to neurodevelopment of infants and children¹⁻³. Copper toxicosis may cause hepatitis, liver cirrhosis, jaundice and hemolytic crisis^{4, 5}. Therefore, heavy metal analysis is imperative and significant for human health care. The methodology of electrochemical analysis demonstrates its outstanding merits in terms of easy operation, simple sample pretreatment and cost-effective instrumentation compared with other approaches such as atomic absorption spectroscopy (AAS), inductively coupled plasma mass spectroscopy (ICP-MS) and atomic fluorescence spectroscopy (AFS).

Electrochemical behaviour of working electrodes is crucial to analysis of specific substance. Besides conventional hanging mercury drop electrodes⁶ and mercury film electrodes^{7, 8}, many environmental-friendly materials have been explored and exploited such as bismuth electrode⁹⁻¹², gold electrode¹³⁻¹⁵ and antimony film electrode^{16, 17}. On the other hand, microscale and nanoscale electrodes demonstrate superior performance to conventional macroscopical electrodes in mass transport rate, signal to noise ratio and sensitivity^{18, 19}. As decreasing in size of electrodes, radial diffusion dominates in the diffusion process, yielding larger mass transport rate. Moreover, higher signal to noise ratio is attained on account of lower charging current resulting from smaller dimension. Various morphological structures of electrodes have been researched including nanoband electrodes²⁰, nanopore electrodes²¹,

1
2
3
4 nanowire electrodes ²² and nanorod electrodes ²³. Among all those electrodes, nanoband
5
6 electrodes are much easier in fabrication than other nanodevices and also offer satisfactory
7
8 scope for nanoscale electrodes in sensing applications ¹⁸.
9

10
11 Light addressable potentiometric sensor (LAPS) is a semiconductor device comprised of a
12
13 heterostructure of silicon/silicon oxide/silicon nitride. LAPS was firstly employed in pH
14
15 detection based on the response of photocurrent induced by illumination of a modulated light.
16
17 Afterwards, many other applications are developed such as cell monitoring ²⁴, heavy metal
18
19 sensing ²⁵ and analyte imaging with high lateral resolution ^{26 27}. It is worth stressing that
20
21 LAPS shows good linearity, sensitivity and stability in pH detection and can be easily
22
23 compatible with other microelectronics facilities ²⁸.
24
25
26
27

28
29 Many related studies about multisensor integration have been explored aiming at enlarging
30
31 practical application of sensors. S. A. Ivanova et al. ²⁹ introduced a pen-like multi-electrode
32
33 potentiometric sensing platform for lead and pH detection, which comprised a seven-in-one
34
35 electrode incorporating ion-selective electrodes and reference electrodes. Robert D. Gardner
36
37 et al. ³⁰ reported a microelectrode array sensing platform combining electrochemical and
38
39 spectrochemical analysis. M. G. Martin et al. ³¹ presented a multisensor system based on three
40
41 different nanowires for detection of antioxidants. Considering the easily compatible property
42
43 of nanoband electrode array (NEA) and LAPS, we designed a miniaturized multisensor chip
44
45 based on NEA for lead and copper detection, together with LAPS for pH sensing in
46
47 electrochemical analysis. Besides, as presented in many studies, the acidity of solutions can
48
49 largely affect the performance of electrochemical analysis through hydrogen evolution,
50
51 hydrolysis of heavy metal and hydroxylation of working electrodes ^{10, 32}. Hence, pH
52
53
54
55
56
57
58
59
60

1
2
3 information provided by LAPS is also meaningful in heavy metal analysis to ensure best
4
5
6 electrochemical performance. Both NEA and LAPS were characterized in detail to ensure the
7
8
9 performance.

10 11 12 **2. Experimental**

13 14 15 **2.1 Chemicals and reagents**

16
17
18 All reagents used in the experiments were of analytical pure grade. De-ionized water
19
20 (>18.2 MΩcm) used for cleaning and dilution was prepared in Mili-Q system (Milipore,
21
22 USA). The standard solutions of lead and copper (100 µg/mL) were purchased from National
23
24 Research Center for Certified Reference Material, China. Other reagents were purchased from
25
26 Aladdin (Shanghai, China). 0.1 M acetate buffer (pH 4.5) was used as the base solution. 1 M
27
28 hydrochloric acid and sodium hydroxide were utilized for pH adjustment in NEA and LAPS
29
30 analysis. Three electrodes system was applied in NEA and LAPS, an external Ag/AgCl
31
32 electrode (saturated KCl) as the reference electrode and a platinum electrode as the counter
33
34 electrode. CHI1030 electrochemical analyser (CH instrument, USA) was used for
35
36 electrochemical analysis of NEA. In SWSV, the parameters were set as follows unless stated
37
38 otherwise: deposition potential -0.6 V, step increment 5 mV, deposition time 120 s, resting
39
40 time 15 s, sampling frequency 25 Hz and sampling amplitude 0.05 V. A potentiostat (Model
41
42 273A, EG&G) was used for I-V-converting and applying the bias voltage to LAPS. The 16 bit
43
44 data acquisition card and the software of LABVIEW were used for LAPS data acquisition and
45
46 analysis. NEA and LAPS tests were carried out in different time to eliminate possible mutual
47
48 interference between the two sensors.
49
50
51
52
53
54
55
56
57
58
59
60

2.2 Multisensor chip fabrication

The miniaturized multisensor chip was fabricated with a series of photolithography methodologies. The detailed parameters for fabrication were selected based on our previous studies³²⁻³⁴. The schematic diagram of detailed fabrication procedures are shown in Fig. 1. A 430 μm N-type silicon wafer with resistivity of 10 Ωcm was designated as the substrate of the sensor and LAPS area was etched to thickness of 100 μm for sufficient light illumination by a modulated LED light in the notch. A SiO_2 layer of 50 nm and Si_3N_4 layer of 20 nm were deposited on the substrate by thermal growth and plasma enhanced chemical vapor deposition (PECVD) in step 2. Specifically fabricated mask was used with photolithography to etch the two layers and pattern the LAPS structure in step 3. The LAPS area of the chip formed consequently with three steps. For the formation of NEA structure, an additional SiO_2 layer of 600 nm was thermally grown on NEA area as the substrate for metallic layer. Besides, the SiO_2 layer with large thickness can reduce the photocurrent yielding in NEA area to a great extent, thus minimizing interferences in LAPS sensing effectively. The metallic layer including a chromium layer of 30 nm and a gold layer of 300 nm was sputtered on the substrate in step 4, in which the chromium layer acted as the adhesion layer. In step 5, the metallic layer was etched to form the NEA structure with isolated gold nanoband electrodes. In step 6 and 7, a SiO_2 layer of 400 nm and Si_3N_4 layer of 400 nm were deposited with PECVD on the metallic layer for insulation and partial insulation areas were etched to expose designated gold area for spot welding to external bonding pad. In the last step, an aluminum layer of 300 nm was vacuum-deposited on the back of LAPS area for LAPS ohmic contact.

Fig.1

NEA and LAPS were integrated on the same chip after all fabrications above, of which the size is 22.2 mm × 12.5 mm. The morphological structure of the sensor is shown in Fig. 2(a). The lateral surface of the chip acts as the working surface of NEA, in which 100 nanoband electrodes compose the array. Partial gold area is designated particularly as the conductor for NEA signal input and acquisition. The whole NEA shares the same welding spot at the rear of the chip. LAPS region (10 mm × 10 mm) is surrounded by gold wire and the Si₃N₄ layer is exploited as the sensitive membrane for pH detection. On the back of LAPS region, an aluminum layer was used for LAPS ohmic contact and a modulated LED was fixed in the notch (circular region of 6 mm diameter) for illumination. The actual photograph of the chip is shown in Fig. 2(b) packaged on a customized printed circuit board. At the bottom of the chip, two bonding pads were used for LED welding and input of modulation signal. The bonding pads at the left side were used for LED, LED, NEA and LAPS connection from bottom, respectively. Optical microscope and scanning electron microscope (SEM) were used for NEA surface characterization presented in Fig. 2(c) and (d). Fig. 2(c) shows that the nanoband electrodes rank neatly in the sensor, of which the size of individual electrode is 8 mm × 6 μm × 300 nm (length × width × thickness). The spacing between individual electrodes is 60 μm, ten times of the width. The surface of lateral side of NEA was characterized and the photograph is shown in (d). No apparently rough region was observed at the surface of NEA and the thickness of gold electrode was confirmed about 350nm, which matches the designated thickness of the metallic layer.

Fig.2

3 Results and discussion

3.1 Characterization of NEA

3.1.1 Cyclic voltammetry analysis

Cyclic voltammetry is a commonly used approach for electrochemical characterization. In this study, cyclic voltammetry was carried out in 0.5 M H₂SO₄ for activation and cleaning of the electrode, thus assuring the electrochemical behaviour preliminarily. After twenty times cyclic scanning from -0.8 V to 1.8 V with scan rate 50 mV/s, cyclic voltammograms remained stable and characteristic curves were acquired for electrochemical analysis. The three replicated voltammograms scanning from 0.2 V to 1.8 V are shown in Fig. 3(a). The voltammograms present good repeatability, indicating satisfactory clean status of the electrode for further voltammetry analysis. Moreover, the oxidation peak (A) and reduction peak (B) of NEA are respectively observed at 1.2 V and 1.0 V during positive and negative scanning, which are in coincidence with the characteristic redox potential of gold electrode.

On the other hand, the working window of the electrode should be evaluated by cyclic voltammetry in order to determinate the scan range and ions species for detection. The working window is dependent on the potential of hydrogen evolution in negative direction and the oxidation potential of electrode in positive direction¹¹. Thus, cyclic voltammetry was conducted in acetate buffer (pH 4.5) scanning from -0.8 V to 1.6 V with scan rate 50 mV/s. As shown in Fig. 3(b), an abrupt change (E) of the curve caused by hydrogen evolution is

1
2
3
4 observed at about -0.6 V in both positive and negative scan. In positive direction, the
5
6 oxidation of NEA (C) starts at about 1.1 V and the reduction of NEA (D) occurs at 0.8 V. That
7
8 is to say, the working window of NEA is confirmed from -0.6 V to 1.1 V summarily and NEA
9
10 can be used for detection of lead and copper regarding to the stripping potential of the two
11
12 heavy metal ions.
13
14

15
16
17
18
19
20
21
22
23
24
25
26
27
28
29
30
31
32
33
34
35
36
37
38
39
40
41
42
43
44
45
46
47
48
49
50
51
52
53
54
55
56
57
58
59
60



Fig.3

3.1.2 Optimum parameters for SWSV

SWSV is widely used in electrochemical analysis due to its capability of decreasing background noise and enhancing signal to noise ratio³⁵. Deposition potential and deposition time are significant parameters for heavy metal detection in SWSV analysis. Therefore, different deposition potential and deposition time were investigated to optimize the parameters in acetate buffer with 100 µg/L lead and copper ions. As shown in Fig. 4(a), the deposition potential varies from -0.8 V to -0.4 V and the corresponding stripping currents are presented. Overall, the stripping current of copper increases as the deposition potential changes positively. The optimum deposition potential is at -0.6 V with best performance for stripping of copper. As for the currents of lead, no significant variation of the stripping current is observed from -0.8 V to -0.5 V, indicating negligible influence of deposition potential to the reduction of lead within the potential scope. Nevertheless, an abrupt decrease of the stripping current arises at -0.4 V ascribing to insufficient deposition of lead. Considering the current variation of lead and copper, -0.6 V was determined as the optimal deposition potential in SWSV analysis.

1
2
3 Different deposition times for SWSV analysis were also studied and plot of stripping
4 current versus deposition time is shown in Fig. 4(b). The overall stripping current increases as
5 the increasing of deposition time. Despite a long deposition time resulting in a high stripping
6 current, time cost during sample analysis and detection range of the electrode should be taken
7 into consideration. The deposition of lead and copper on the working electrode can be easily
8 saturated under conditions with long deposition time and high concentration. Thus, deposition
9 time was set to be 120 s with optimum performance.
10
11
12
13
14
15
16
17
18
19

20
21
22
23
24
25
26
27
28
29
30
31
32
33
34
35
36
37
38
39
40
41
42
43
44
45
46
47
48
49
50
51
52
53
54
55
56
57
58
59
60

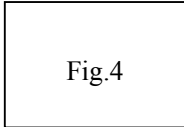


Fig.4

The acidity of solutions is another critical condition significantly affecting the electrochemical process for heavy metal analysis. Herein, we discussed the influence of different pH to the analysis of lead and copper. Hydrochloric acid and sodium hydroxide were used for pH adjustment in acetate buffer with 100 $\mu\text{g/L}$ lead and copper ions. The voltammograms are shown in Fig. 5 (a) with pH varying from 2 to 7. Well-defined stripping peaks of lead and copper are observed at around -0.4V and -0.06V under conditions of pH 2, 3 and 4, while abrupt decreases of stripping peaks occur in pH 4.5 and 5, especially for peaks of copper. As the solution adjusting to more alkaline, the stripping peaks of lead and copper turn negligible and no significant oxidation peaks can be observed. The peak currents of lead and copper were extracted and plot of stripping current versus pH is presented in Fig. 5 (b). Overall, the peak currents of lead and copper reduce as decreasing of the acidity of solution, which attributes to a decreasing sensitivity of NEA and the increasing hydrolysis of heavy metal ions. Under conditions of pH 6 and 7, the peak currents decrease below μA level, which

1
2
3
4 is unsuitable for heavy metal analysis. It is evident that the acidity of the solution affects the
5
6 performance of NEA for heavy metal analysis to a great extent. Thus, pH information
7
8 provided by LAPS is very meaningful to guarantee the appropriate acidity in electrochemical
9
10 analysis. To assure a higher electrochemical response, further experiments were carried out in
11
12 solutions of pH 2.
13
14

15
16
17
18
19
20
21
22
23
24
25
26
27
28
29
30
31
32
33
34
35
36
37
38
39
40
41
42
43
44
45
46
47
48
49
50
51
52
53
54
55
56
57
58
59
60



Fig.5

3.1.3 Heavy metal analysis with SWSV

After activation and cleaning of NEA in sulfuric acid, quantitative analysis of lead and copper was conducted with SWSV and standard addition method in acetate buffer. The acidity of the solution was adjusted to pH 2 with deposition potential -0.6 V and deposition time 120 s as summarized above. 20 µg/L lead and copper ions were added in each addition. Plots of stripping voltammograms versus scan potential under different heavy metal concentrations are shown in Fig. 6 (a). The characteristic stripping potentials of lead and copper are at around -0.39 V and -0.08 V, respectively. Apparent gradient of peak currents is observed as increasing of the concentration ranging from 20 ppb to 100 ppb. The peak currents of lead and copper were extracted and plot of peak current versus concentration is presented in Fig. 6 (b). The calibration equation of lead is $I_{Pb}=0.510\pm0.046C+9.945$ with correlation coefficient of 0.9767 and sensitivity of 0.510 ± 0.046 µA/ppb, while the linear calibration equation of copper is $I_{Cu}=0.678\pm0.017C+8.156$ with correlation coefficient of 0.9982 and sensitivity of 0.678 ± 0.017 µA/ppb. Besides, detection range of NEA for lead and copper was investigated as well. The experiments indicate that the sensor has a good linear response in the range of

0-500 ppb for both lead and copper. For higher concentration of heavy metal ions, the sensitivity of NEA decreases due to the saturation of the sensor.

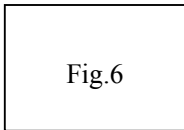


Fig.6

The reproducibility and long-term stability of NEA were also investigated to assess the performance for detection of lead and copper. Experiments were carried out in acetate buffer (pH 2) with Pb 100 $\mu\text{g/L}$ and Cu 100 $\mu\text{g/L}$. The five replicated stripping currents in a short time are shown in Fig. 7 (a). The relative standard deviations (RSD) of lead and copper are 6.3% and 2.8%, respectively, indicating good reproducibility of the sensor. On the other hand, long-term detection within five hour was also experimented shown in Fig. 7(b) with a RSD of lead 16.2% and copper 2.0%, respectively. A relatively large RSD was observed in both repetitive and long-term detection of lead, which could be ascribed to the oxidation potential of lead adjacent to hydrogen evolution. Unstable hydrogen evolution reaction affects the electrochemical performance of gold NEA for lead analysis. As a comparison, gold NEA exhibits reasonably excellent reproducibility and long-term stability for copper detection.

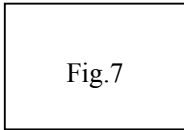


Fig.7

Interferences from other ion species were also discussed. Experiments were also carried out in acetate buffer (pH 2) with Pb 100 $\mu\text{g/L}$ and Cu 100 $\mu\text{g/L}$. General ions including Na^+ , K^+ , Ca^{2+} , Mg^{2+} , Cl^- , NO_3^- and SO_4^{2-} were studied and the results suggested that 10-fold external ions could make interferences less than 8% on lead and copper detection. 10-fold Zn^{2+} was especially studied due to Zn-Cu intermetallic compound mentioned in many studies ^{36, 37}.

1
2
3
4 However, additional Zn^{2+} made no significant influence on the stripping peak of copper and
5
6 the explanation is that the deposition potential is -0.6 V, below the reduction potential of zinc.
7
8
9 No Zn-Cu intermetallic compound could form thereby.

10 11 12 **3.2 Characterization of LAPS**

13
14
15 The electrochemical behaviour of LAPS was experimented to characterize the performance
16
17 in terms of its linearity, sensitivity and reproducibility. The LED fixed for illumination with
18
19 the wavelength of 650 nm was modulated at an alternating current (I_{p-p} 10mA, frequency 10k
20
21 Hz). The scanning range was set from -500 mV to 2000 mV, with one step increment of 10mV.
22
23 Plots of photocurrent versus bias potential (I-V) are presented in Fig. 8 with pH ranging from
24
25 3 to 7.9. As shown in the figure, the I-V curve shifts significantly to positive direction with
26
27 pH varying from acidity to alkalinity. The saturation region and cut-off region of the curves
28
29 are well coincident under different pH circumstances, beneficial for further quantitative
30
31 analysis and extraction of working points. As to quantify the shift of curves, we sought
32
33 intersection points from the curves and a constant photocurrent. Herein, we designated the
34
35 intersection points with constant photocurrent 2000 nA as working points to characterize the
36
37 shift of potential. Considering the insufficient sampling frequency of single data per 10 mV,
38
39 linear interpolation was applied to enhance the accuracy of calculated potential.
40
41 Corresponding characteristic potential values were extracted and employed for calibration. As
42
43 shown in Fig. 8(b), plot of potential versus pH has a high correlation coefficient of 0.9999,
44
45 indicating a good pH linearity of the sensor. The calibration equation is $V=56.49pH+83.61$
46
47 with high sensitivity of 56.49 mV/pH, which is well consistent with the Nernst equation for
48
49 monovalent ion.
50
51
52
53
54
55
56
57
58
59
60

Fig.8

The reproducibility of LAPS was also investigated in samples. Each sample was measured for three times and the three repetitive I-V curves of pH 3 and 4 were mainly discussed. As shown in Fig. 9, the three repetitive curves of both pH 3 and 4 are almost entirely overlapped. The working points in photocurrent of 2000 nA were also extracted to evaluate the reproducibility as shown in the inset. Three I-V curves with deviation less than 2 mV were attained both in pH 3 and 4, indicating good reproducibility for pH analysis. LAPS on the multisensor chip exhibits excellent linearity, sensitivity and reproducibility for pH analysis in solutions, which can offer accurate pH information for electrochemical analysis.

Fig.9

3.3 Comparisons

The presented multisensor chip is a simplification and improvement to our previous fabricated integrated sensor³². The multisensor chip is fabricated with NEA and LAPS integration, demonstrating higher sensitivity and smaller size, while the previous sensor is integrated with several MEAs and LAPSs. Thus, better performance is obtained in the multisensor chip in heavy metal determination. Besides, no specific working cell is required when utilizing the multisensor chip, while the integrated sensor is packaged on the bottom of a working cell, inconvenient for replacement and causing higher cost. And the lateral working surface of the multisensor chip is also convenient for sensor renewal. However, surface modification is difficult to apply on NEA due to the nanoscale size of the surface, which

1
2
3 restricts the measurable ion species. External reference and counter electrodes are required
4
5
6 when utilizing the chip.
7
8

9 10 **4. Conclusion**

11
12
13 We presented a miniaturized multisensor chip based on NEA for lead and copper detection,
14
15 together with LAPS for pH sensing. The working window of NEA was characterized from
16
17 -0.6 V to 1.1 V. Deposition potential and deposition time were optimized to be -0.6 V and 120
18
19 s with best electrochemical performance. The acidity of the solution was confirmed to largely
20
21 restrict the electrochemical behaviour of NEA and pH 2 was selected as the best condition for
22
23 heavy metal detection. With the optimized parameters, NEA exhibited outstanding linearity,
24
25 sensitivity, reproducibility and long-term stability for heavy metal detection. LAPS on the
26
27 chip also showed satisfactory linearity, sensitivity and reproducibility for pH detection.
28
29 Besides, based on pH information provided by LAPS, NEA can be guaranteed to work in
30
31 solutions with appropriate acidity, which is beneficial to obtain the best electrochemical
32
33 response. On the other hand, three-electrode system integration could be implemented on the
34
35 same chip similar to screen-printed electrodes^{38,39}, which is promising in our future work.
36
37
38
39
40
41
42
43

44 **Acknowledgement**

45
46
47 This work was supported by National 973 Project (No. 2015CB352101) and Marine Public
48
49 Welfare Project of China (No. 201305010).
50
51

52 **References**

- 53
54
55
56 1. L. Patrick, *Altern. Med. Rev.*, 2006, **11**, 2-22.
57
58 2. A. Navas-Acien, E. Guallar, E. K. Silbergeld and S. J. Rothenberg, *Environ Health Persp*,
59 15
60

- 2007, 472-482.
3. G. Flora, D. Gupta and A. Tiwari, *Interdisciplinary toxicology*, 2012, **5**, 47-58.
 4. L. M. Gaetke and C. K. Chow, *Toxicology*, 2003, **189**, 147-163.
 5. B. R. Stern, *Journal of Toxicology and Environmental Health, Part A*, 2010, **73**, 114-127.
 6. M. Ghoneim, A. Hassanein, E. Hammam and A. Beltagi, *Fresenius J. Anal. Chem.*, 2000, **367**, 378-383.
 7. M. F. de Oliveira, A. A. Saczk, L. L. Okumura, A. P. Fernandes, M. de Moraes and N. R. Stradiotto, *Anal. Bioanal. Chem*, 2004, **380**, 135-140.
 8. E. Fischer and C. M. van den Berg, *Anal Chim Acta*, 1999, **385**, 273-280.
 9. J. Wang, *Electroanalysis*, 2005, **17**, 1341-1346.
 10. Z. Bi, C. S. Chapman, P. Salaün and C. M. van den Berg, *Electroanalysis*, 2010, **22**, 2897-2907.
 11. Z. Zou, A. Jang, E. Macknight, P.-M. Wu, J. Do, P. L. Bishop and C. H. Ahn, *Sens. Actuator B-Chem*, 2008, **134**, 18-24.
 12. J. Wang, J. Lu, S. B. Hocevar, P. A. Farias and B. Ogorevc, *Anal Chem*, 2000, **72**, 3218-3222.
 13. S. Laschi, I. Palchetti and M. Mascini, *Sens. Actuator B-Chem*, 2006, **114**, 460-465.
 14. E. Bernalte, C. M. Sánchez and E. P. Gil, *Anal Chim Acta*, 2011, **689**, 60-64.
 15. G. M. Alves, J. M. Magalhães, P. Salaün, C. M. Van den Berg and H. M. Soares, *Anal Chim Acta*, 2011, **703**, 1-7.
 16. V. Urbanová, K. Vytrás and A. Kuhn, *Electrochem Commun*, 2010, **12**, 114-117.
 17. E. Svobodova-Tesarova, L. Baldrianova, M. Stoces, I. Svancara, K. Vytras, S. B. Hocevar and B. Ogorevc, *Electrochim Acta*, 2011, **56**, 6673-6677.
 18. D. W. Arrigan, *Analyst*, 2004, **129**, 1157-1165.
 19. X. Xie, D. Stüben, Z. Berner, J. Albers, R. Hintsche and E. Jantzen, *Sens. Actuator B-Chem*, 2004, **97**, 168-173.
 20. A. Mardegan, S. Dal Borgo, P. Scopece, L. Moretto, S. B. Hocevar and P. Ugo, *Electrochem Commun*, 2012, **24**, 28-31.
 21. J.-F. Huang and B.-T. Lin, *Analyst*, 2009, **134**, 2306-2313.
 22. N. Tzamtzis, V. N. Psychoyios, G. P. Nikoleli, D. P. Nikolelis, N. Psaroudakis, M. Willander and M. Qadir Israr, *Electroanalysis*, 2012, **24**, 1719-1725.

- 1
2
3
4
5
6
7
8
9
10
11
12
13
14
15
16
17
18
19
20
21
22
23
24
25
26
27
28
29
30
31
32
33
34
35
36
37
38
39
40
41
42
43
44
45
46
47
48
49
50
51
52
53
54
55
56
57
58
59
60
23. Z. H. Ibupoto, N. Mitrou, G. P. Nikoleli, D. P. Nikolelis, M. Willander and N. Psaroudakis, *Electroanalysis*, 2014, **26**, 292-298.
24. N. Hu, C. Wu, D. Ha, T. Wang, Q. Liu and P. Wang, *Biosens Bioelectron*, 2013, **40**, 167-173.
25. D. Ha, N. Hu, C. X. Wu, D. Kirsanov, A. Legin, M. Khaydukova and P. Wang, *Sens. Actuator B-Chem*, 2012, **174**, 59-64.
26. T. Yoshinobu, H. Iwasaki, Y. Ui, K. Furuichi, Y. Ermolenko, Y. Mourzina, T. Wagner, N. Näther and M. Schöning, *Methods*, 2005, **37**, 94-102.
27. K.-i. Miyamoto, T. Wagner, T. Yoshinobu, S. i. Kanoh and M. J. Schöning, *Sens. Actuator B-Chem*, 2011, **154**, 28-32.
28. Q. Liu and P. Wang, *Cell-based biosensors: principles and applications*, Artech House, 2009.
29. S. Anastasova-Ivanova, U. Mattinen, A. Radu, J. Bobacka, A. Lewenstam, J. Migdalski, M. Danielewski and D. Diamond, *Sens. Actuator B-Chem*, 2010, **146**, 199-205.
30. R. D. Gardner, A. Zhou and N. A. Zufelt, *Sens. Actuator B-Chem*, 2009, **136**, 177-185.
31. M. Gay Martín, J. A. de Saja, R. Muñoz and M. L. Rodríguez-Méndez, *Electrochim Acta*, 2012, **68**, 88-94.
32. H. Wan, D. Ha, W. Zhang, H. Zhao, X. Wang, Q. Sun and P. Wang, *Sens. Actuator B-Chem*, 2014, **192**, 755-761.
33. H.-X. Zhao, W. Cai, D. Ha, H.-S. Guo and P. Wang, *Sensor Letters*, 2011, **9**, 801-806.
34. N. Hu, D. Ha, C. Wu, J. Zhou, D. Kirsanov, A. Legin and P. Wang, *Sensors and Actuators A: Physical*, 2012, **187**, 50-56.
35. X.-s. Zhu, C. Gao, J.-W. Choi, P. L. Bishop and C. H. Ahn, *Lab. Chip*, 2005, **5**, 212-217.
36. J. Wang, J. Lu, Ü. A. Kirgöz, S. B. Hocevar and B. Ogorevc, *Anal Chim Acta*, 2001, **434**, 29-34.
37. E. Shams, A. Babaei and M. Soltaninezhad, *Anal Chim Acta*, 2004, **501**, 119-124.
38. M. Li, Y.-T. Li, D.-W. Li and Y.-T. Long, *Anal Chim Acta*, 2012, **734**, 31-44.
39. H. Wan, Q. Sun, H. Li, F. Sun, N. Hu and P. Wang, *Sens. Actuator B-Chem*, 2015, **209**, 336-342.

Figure Captions

Figure 1: The schematic diagram of detailed fabrication procedures for the multisensor chip:

(1) Silicon etching. (2) SiO₂ and Si₃N₄ deposition. (3) LAPS photoetching and SiO₂ deposition. (4) Metallic layer deposition. (5) NEA photoetching. (6) Insulation layer deposition. (7) Insulation layer photoetching. (8) Aluminum deposition.

Figure 2: The morphological structure of the fabricated sensor (a) and the packaged sensor with PCB (b). The microstructure and lateral surfaces of NEA are shown in (c) and (d) with optical microscopy and scanning electron microscopy.

Figure 3: The cyclic voltammograms of NEA in 0.5 M H₂SO₄ (a) for activation and 0.1 M pH 4.5 acetate buffer (b) for assuring the working window with scan rate 50 mV/s.

Figure 4: The current response of NEA with different deposition potential (a) from -0.8 V to -0.4 V (vs. Ag/AgCl) and deposition time (b) from 30 s to 180 s.

Figure 5: Plots of voltammograms under different solutions from pH 2 to 7 (a) and stripping peak current versus pH (b) to evaluate effects of pH variation.

1
2
3
4 Figure 6: Plots of stripping voltammograms versus scan potential (vs. Ag/AgCl) under
5
6 different heavy metal concentrations from 20 ppb to 100 ppb (a). The calibrations of lead and
7
8 copper are shown in (b).
9

10
11
12
13
14 Figure 7: The reproducibility and long-term stability of NEA for lead and copper detection: (a)
15
16 stripping currents in five replicated tests; (b) stripping currents in five hours tests.
17
18

19
20
21 Figure 8: Plots of photocurrent versus bias potential (vs. Ag/AgCl) from pH 3 to 7.9 (a) and
22
23 the calibration curve of characteristic potential versus pH (b).
24
25

26
27
28
29 Figure 9: The three repetitive tests of LAPS in pH 3 and pH 4 solutions and zoomed area in
30
31 characteristic potential range.
32
33
34
35
36
37
38
39
40
41
42
43
44
45
46
47
48
49
50
51
52
53
54
55
56
57
58
59
60

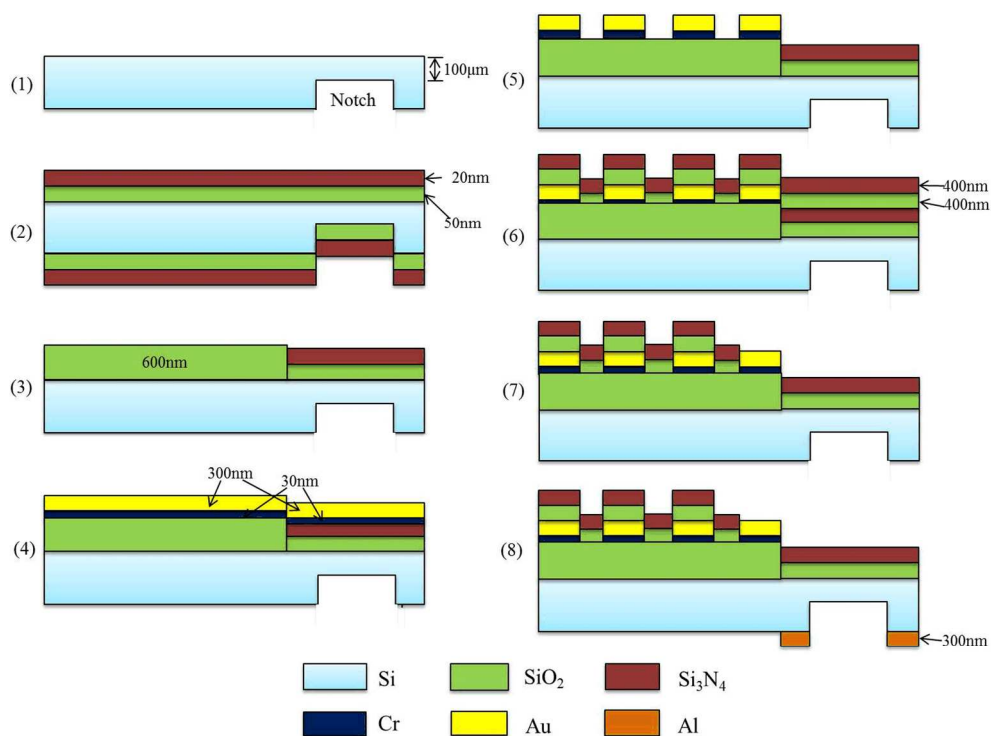


Figure 1. The schematic diagram of detailed fabrication procedures for the multisensor chip: (1) Silicon etching. (2) SiO₂ and Si₃N₄ deposition. (3) LAPS photoetching and SiO₂ deposition. (4) Metallic layer deposition. (5) NEA photoetching. (6) Insulation layer deposition. (7) Insulation layer photoetching. (8) Aluminum deposition.
258x190mm (300 x 300 DPI)

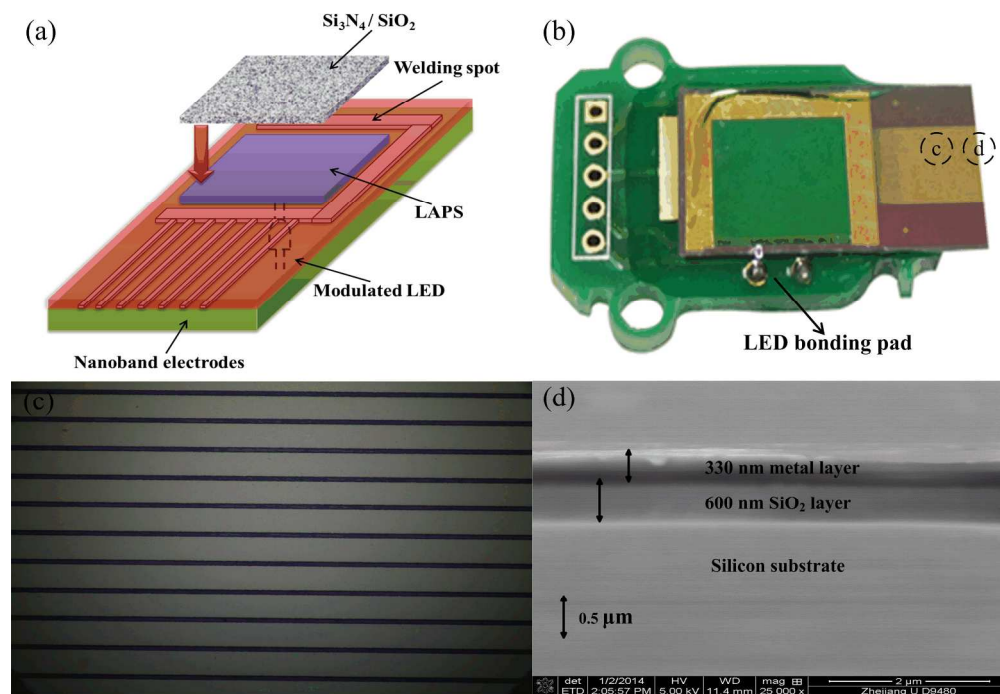


Figure 2. The morphological structure of the fabricated sensor (a) and the packaged sensor with PCB (b). The microstructure and lateral surfaces of NEA are shown in (c) and (d) with optical microscopy and scanning electron microscopy. 223x155mm (300 x 300 DPI)

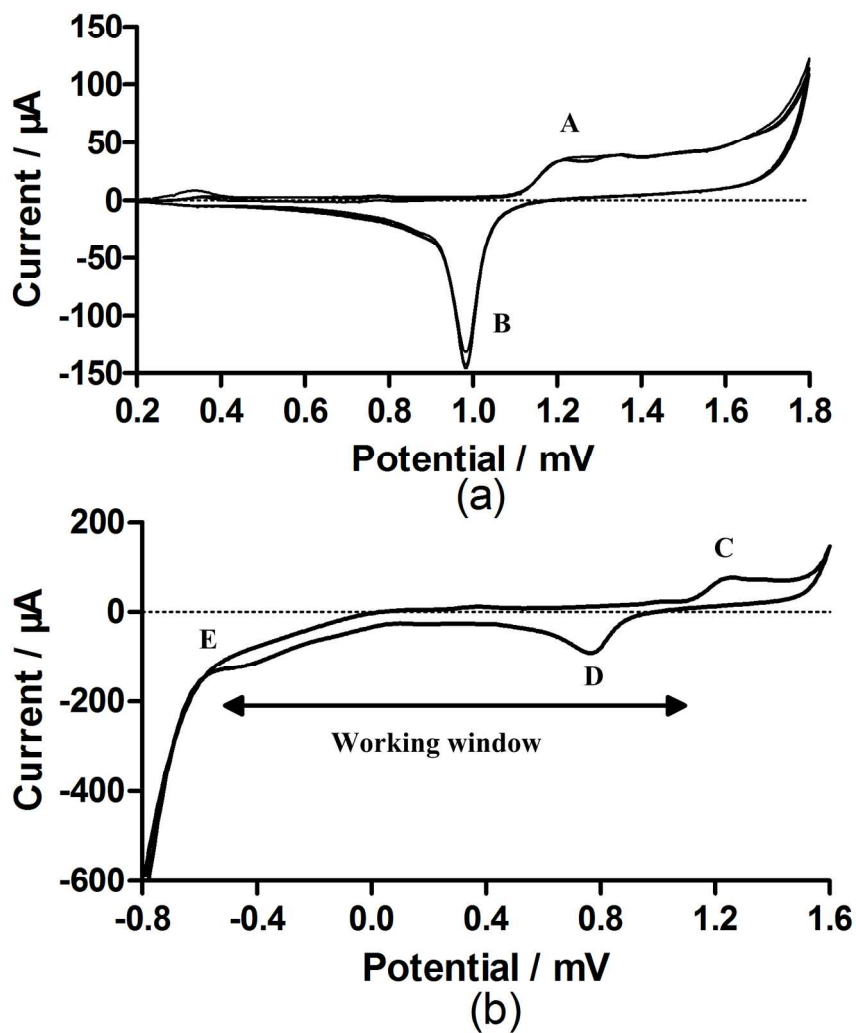


Figure 3. The cyclic voltammograms of NEA in 0.5 M H₂SO₄ (a) for activation and 0.1 M pH 4.5 acetate buffer (b) for assuring the working window with scan rate 50 mV/s
174x201mm (300 x 300 DPI)

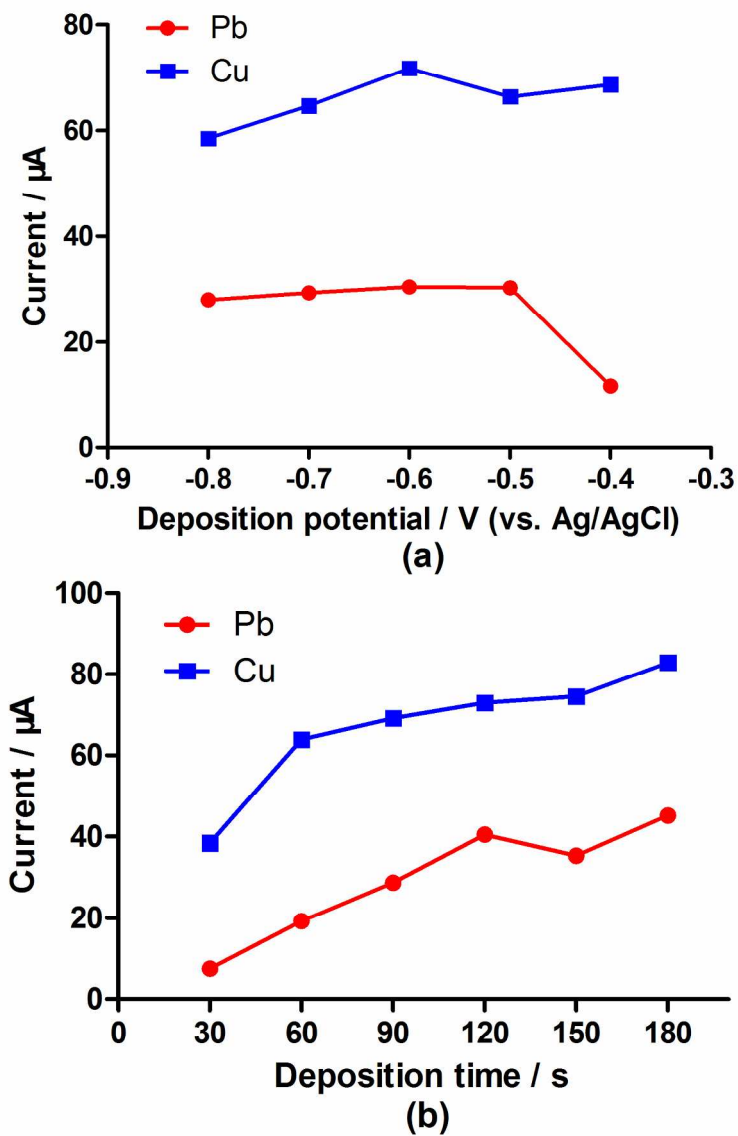


Figure 4. The current response of NEA with different deposition potential (a) from -0.8 V to -0.4 V (vs. Ag/AgCl) and deposition time (b) from 30 s to 180 s.
175x238mm (300 x 300 DPI)

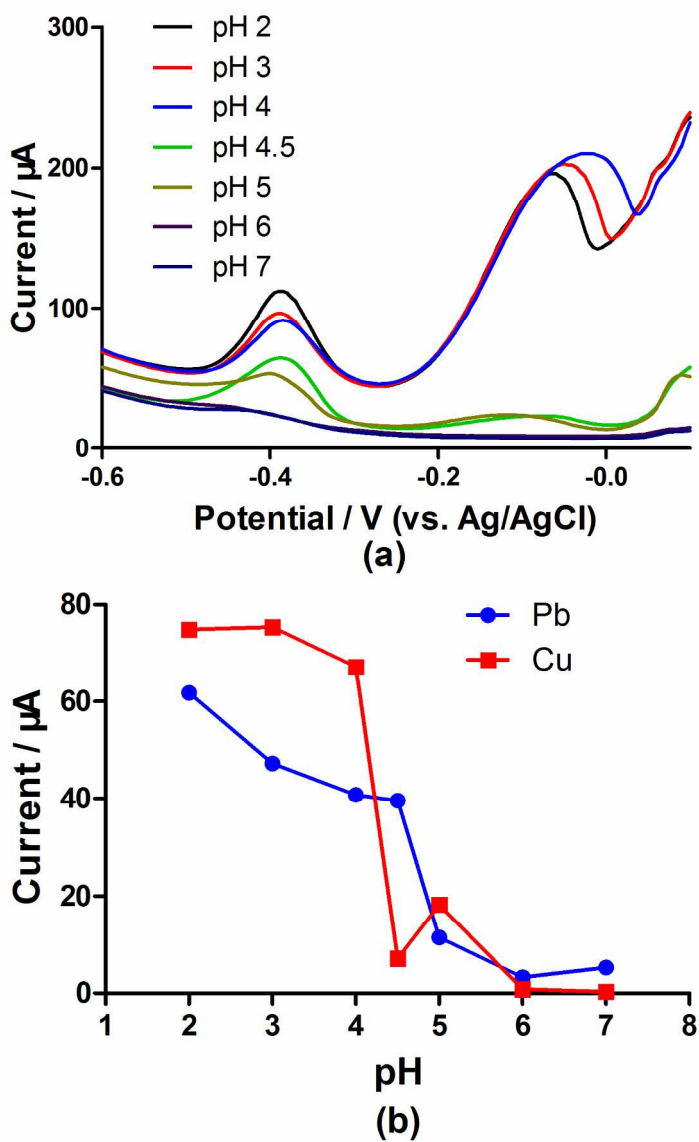


Figure 5. Plots of voltammograms under different solutions from pH 2 to 7 (a) and stripping peak current versus pH (b) to evaluate effects of pH variation.
163x234mm (300 x 300 DPI)

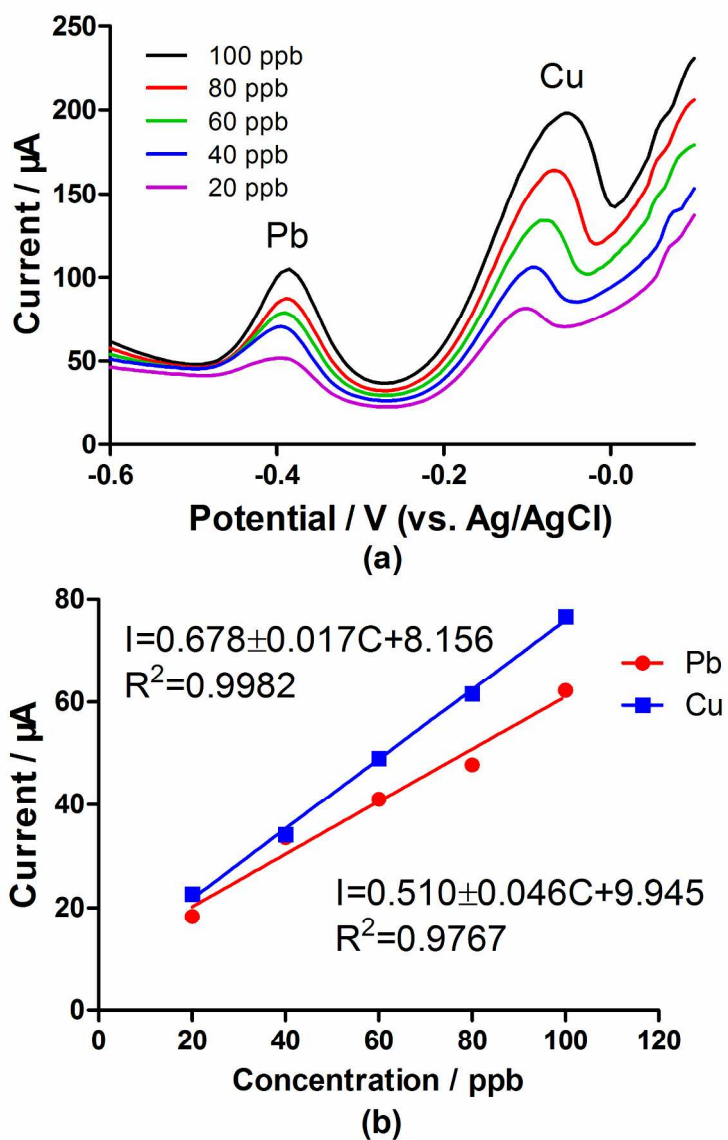


Figure 6. Plots of stripping voltammograms versus scan potential (vs. Ag/AgCl) under different heavy metal concentrations from 20 ppb to 100 ppb (a). The calibrations of lead and copper are shown in (b).
178x256mm (300 x 300 DPI)

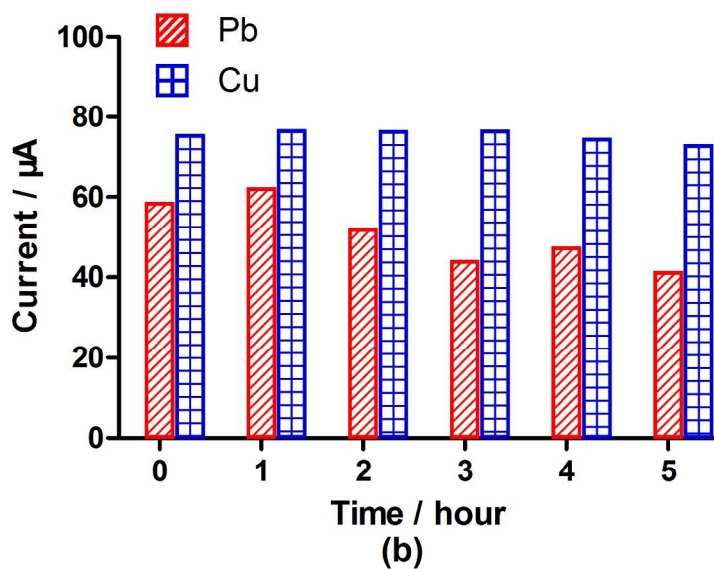
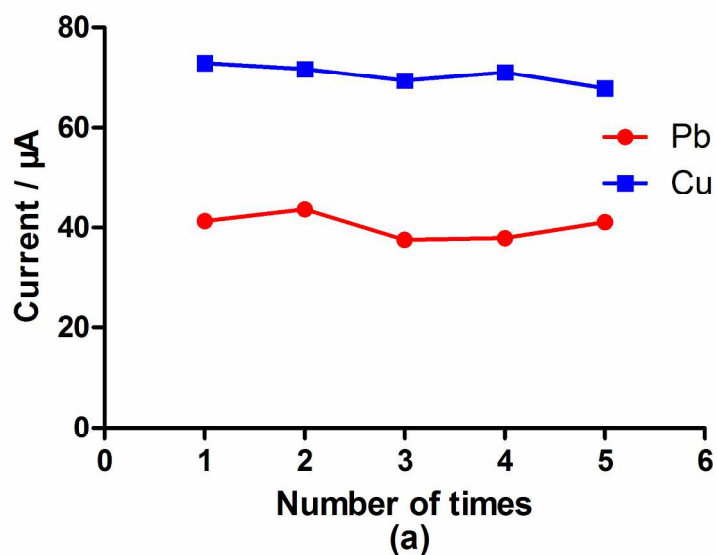


Figure 7. The reproducibility and long-term stability of NEA for lead and copper detection: (a) stripping currents in five replicated tests; (b) stripping currents in five hours tests.
180x249mm (300 x 300 DPI)

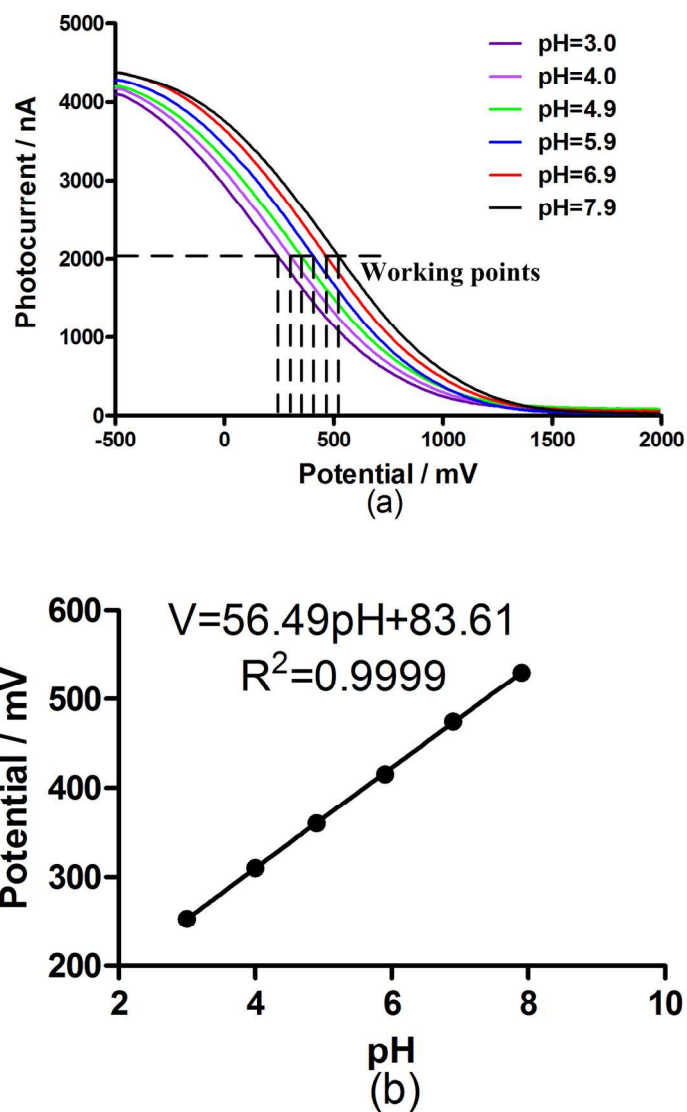


Figure 8. Plots of photocurrent versus bias potential (vs. Ag/AgCl) from pH 3 to 7.9 (a) and the calibration curve of characteristic potential versus pH (b).
155x220mm (300 x 300 DPI)

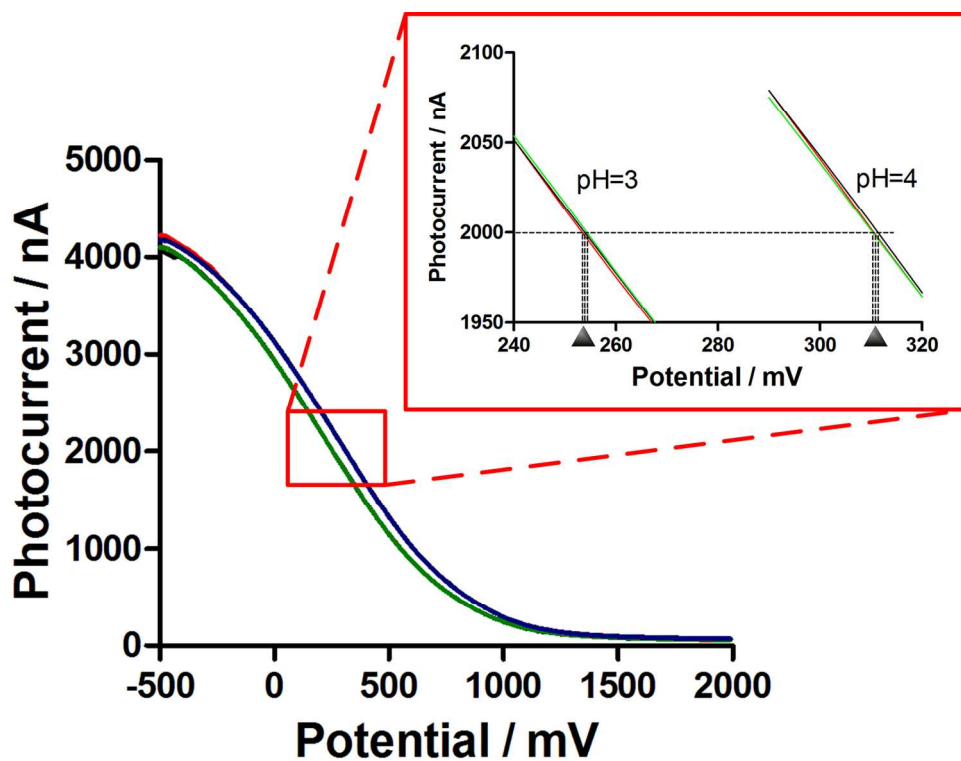
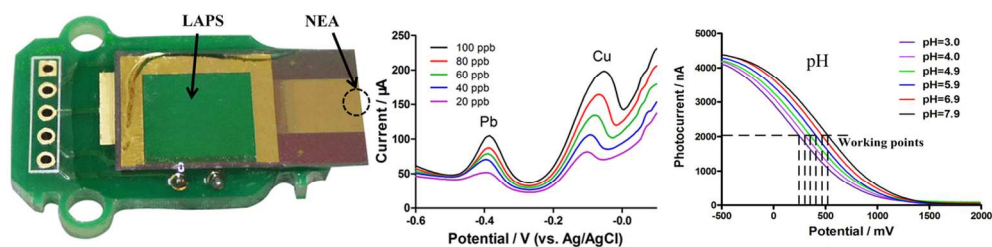


Figure 9: The three repetitive tests of LAPS in pH 3 and pH 4 solutions and zoomed area in characteristic potential range.
154x121mm (300 x 300 DPI)



The photography of the multisensor chip (left), the stripping voltammograms of NEA with different concentrations of lead and copper (middle) and the I-V curves of LAPS in different pH solutions (right).
121x38mm (300 x 300 DPI)